Autofocusing of THz SAR Images by Integrating Compressed Sensing into the Backprojection Process

Yevhen Ivanenko, Viet T. Vu, and Mats I. Pettersson
Department of Mathematics and Natural Sciences, Blekinge Institute of Technology, 37179 Karlskrona, Sweden
{yevhen.ivanenko,viet.thuy.vu,mats.pettersson}@bth.se

***Abstract*—The THz frequency spectrum provides an opportunity to explore high-resolution synthetic-aperture-radar (SAR) short-range imaging that can be used for various applications. However, the performance of THz SAR imaging is sensitive to phase errors that can be caused by an insufficient amount of data samples for image formation and by path deviations that can be practically caused by SAR platform vibrations, changes in speed, changes in direction, and acceleration. To solve the former problem, an improved interpolation procedure for backprojection algorithms has been proposed. However, to make these algorithms efficient in handling the latter problem, an additional autofocusing is necessary.**

In this paper, we introduce an autofocusing procedure based on compressed sensing that is incorporated into the backprojection algorithm. The reconstruction is based on the following calculated parameters: windowed interpolation sinc kernel, and range distances between SAR platform and image pixels in a defined image plane. The proposed approach is tested on real data, which was acquired by the 2πSENSE FMCW SAR system through outdoor SAR imaging.

***Index Terms*—FMCW SAR, THz, Autofocusing, Compressed Sensing**

I. Introduction

Exploration of THz frequencies provides opportunities for the realization of new applications in future 6G systems. One of the potential applications is short-range high-resolution remote sensing, which is of great interest in the area of logistics, security, indoor imaging, etc. To perform remote sensing with high resolution, the synthetic aperture radar (SAR) principle can be used.

SAR technology takes its origin in the 1950s when the objective was to create an alternative to optical imaging systems. The main advantage of the synthetic aperture is that it can be much larger than the aperture of a physical antenna, which results in high-resolution imaging in the cross-range direction.

THz SAR imaging is an interesting research topic. The aim of THz SAR imaging is to design an imaging system that can be mounted on various dynamic platforms. The current state-of-the-art THz SAR systems include ground- and rail-based realizations. Different pulse THz SAR testbeds have been developed to perform high-resolution imaging at frequencies starting from 0.22 THz and up to 1.1 THz; see references [1]–[6] for details. Furthermore, THz SAR systems based on FMCW radars operating in different frequency ranges have emerged, e.g., $[0.122;\ 0.17]$ THz for the system reported in [7], and $[0.126;\ 0.182]$ THz for the system done in [8], [9].

The performance of THz SAR imaging systems is sensitive to phase errors. Practically, phase errors occur due to path deviations, which can be caused by platform vibrations, speed variations of SAR platforms, accelerations, etc. To handle this issue, the backprojection algorithms [10]–[12] are natural solutions for THz SAR imaging systems due to their internal motion-compensation procedure, which is efficient if the deviation information is a priori known. The major computational burden of the backprojection algorithms is the interpolation procedure, the accuracy of which correlates with the upsampling procedure of the raw data. In [13] and [9], an improved interpolation procedure was introduced to process pulse THz SAR and FMCW THz SAR signals. The developed interpolators provide the opportunity to obtain accurate images without upsampling of raw data. However, if the path deviation is unknown, an additional motion-compensation procedure as an add-on to the backprojection algorithms is necessary. This refers to autofocusing.

In [14], Ash introduced an autofocusing algorithm based on the maximization of image sharpness to process spotlight SAR data as an add-on to the backprojection algorithm. Wei et al. in [15] applied the maximum sharpness approach for 3D imaging based on the fast backporjection algorithm. Sommer and Ostermann in [16] proposed to divide a reconstructed image into subimages, and then use the maximum sharpness principle to estimate phase errors on the subimage level. In [17], Torgrimsson et al. introduced a factorized geometrical autofocusing algorithm for processing spotlight or stripmap ultrawideband-ultrawidebeam SAR data, which was integrated into the fast factorized backprojection algorithm. Shi et al. in [18] recently proposed an algorithm for phase error estimation for THz SAR based on the basis pursuit denoise algorithm in the unconstrained form. The algorithm is considered as a support to the range migration algorithm. Despite the algorithm demonstrating good results, the choice of the regularization coefficient in the optimization problem and the absence of an opportunity to perform autofocusing for images, the azimuthal coordinates of which do not agree with the azimuthal coordinates of the SAR aperture, are challenging.

This work was supported by the ELLIIT research environment under the project Multistatic High-resolution Sensing at THz, Project-ID A17.

In this paper, we propose an autofocusing algorithm based on compressed sensing, which is incorporated into the back-projection algorithm as a natural extension. The algorithm eliminates phase errors based on the optimization procedure for a single range bin. The components of the backprojection algorithm, such as the interpolation sinc kernel and range distance between the SAR platform and a point in the image plane, are used under the construction of the sensing matrix.

The rest of the paper is organized as follows: In Section II, the problem setup and the image formation algorithm are described. Section III proposes the autofocusing algorithm. The experimental results are presented in Section IV, and Section V concludes the paper.

II. Problem setup

A. FMCW SAR

Consider a setup for two-dimensional monostatic SAR imaging, which is based on an FMCW radar. The radar transmits the frequency-modulated continuous wave signal, the mathematical representation of which is given by

$$s_{\mathrm{TX}}(t) = \mathrm{e}^{\mathrm{j}2\pi(f_{\min}t+\kappa t^2/2)}, \qquad 0 \le t \le T, \tag{1}$$

where $f_{\min}$ is the start frequency of the emitted frequency ramp, t the range time, κ and T are the slope and the duration of the emitted frequency ramp, respectively.

Suppose that there is a scatterer in the SAR scene under illumination. Then, the signal received by the FMCW SAR system due to the scatterer is expressed as

$$s_{\mathrm{RX}}(\xi,t) = \mathrm{e}^{\mathrm{j}2\pi[f_{\min}(t-2R/\mathrm{c}_0)+\kappa(t-2R/\mathrm{c}_0)^2/2]}, \tag{2}$$

where $2R/\mathrm{c}_0$ is the range-time delay, where c_0 denotes the speed of light in vacuum and the range distance R is given by

$$R = \sqrt{(v\tau-\xi)^2+(\rho'-\rho)^2}. \tag{3}$$

It is obvious that R depends on the corresponding azimuthal and range coordinates of the FMCW SAR platform and the scatterer, i.e., on $(v\tau,\rho')$ and (ξ,ρ), respectively. Note that the azimuthal coordinate of the FMCW SAR system depends on the azimuthal time τ, as well as on the speed of the platform v. The received signal is then down-converted to the intermediate frequency (IF) domain via the mixture procedure of the transmitted and received signals

$$s_{\mathrm{IF}}(\xi,t) = s_{\mathrm{TX}}(t)\overline{s_{\mathrm{RX}}(\xi,t)} = \mathrm{e}^{\mathrm{j}4\pi(f(t)R/\mathrm{c}_0-\kappa(2R/\mathrm{c}_0)^2/2)} \approx \mathrm{e}^{\mathrm{j}4\pi f(t)R/\mathrm{c}_0}, \tag{4}$$

where $f(t) = f_{\min}+\kappa t$ so that $f_{\min} \le f(t) \le f_{\max}$ for $t \in [0,T]$. It should be highlighted that the second term under the exponential operator can be neglected because of $f(t)R/\mathrm{c}_0 \gg \kappa(2R/\mathrm{c}_0)^2/2$ for short-range distances. The down-conversion procedure (4) ensures proper sampling of the received signal.

To obtain signals in the range compressed form, one needs to take first the Fourier transform of the IF signals (4), assuming that the envelope of the IF signal is the rectangular window:

$$S_{\mathrm{IF}}(\xi,f) = \mathcal{F}\{s_{\mathrm{IF}}(\xi,t)\} = T\,\mathrm{sinc}[\pi T(f-\kappa 2R/\mathrm{c}_0)] \times \mathrm{e}^{\mathrm{j}2\pi(f-\kappa 2R/\mathrm{c}_0)\frac{T}{2}}\mathrm{e}^{\mathrm{j}4\pi f_{\min}R/\mathrm{c}_0}, \tag{5}$$

Here, the relation $\kappa 2R/\mathrm{c}_0$ corresponds to the beat frequency f_{b}, from which the range can be estimated as

$$R = \frac{\mathrm{c}_0 T f_{\mathrm{b}}}{2B}. \tag{6}$$

Then, to eliminate the exponential term containing the start frequency $f_{\min}$, the following phase correction procedure can be applied:

$$\tilde{S}_{\mathrm{IF}}(\xi,f) = S_{\mathrm{IF}}(\xi,f)\mathrm{e}^{-\mathrm{j}4\pi f_{\min}R/\mathrm{c}_0} = T\,\mathrm{sinc}[\pi T(f-\kappa 2R/\mathrm{c}_0)]\mathrm{e}^{\mathrm{j}2\pi(f-\kappa 2R/\mathrm{c}_0)\frac{T}{2}}. \tag{7}$$

Finally, by converting the beat frequency to the range and replacing the frequency variable f, it is possible to obtain the range-compressed signal.

In the presence of multiple scatterers in the scene under illumination, the representation of the phase-corrected IF signal can be generalized by employing Born's approximation:

$$\tilde{S}_{\mathrm{IF}}(\xi,f) \approx \sum_{j=1}^{K} T\,\mathrm{sinc}[\pi T(f-\kappa 2R_j/\mathrm{c}_0)]\mathrm{e}^{\mathrm{j}2\pi(f-\kappa 2R_j/\mathrm{c}_0)\frac{T}{2}}. \tag{8}$$

Here, $2R_j/\mathrm{c}_0$ denotes the round time needed for a signal to be transmitted from the FMCW SAR aperture antenna to the corresponding j-th target and backwards, and $K \ge 1$. It should be noted that the range-compressed signal can be obtained by performing a similar procedure as for a single scatterer in the scene under illumination, as described above.

B. Image Formation

Let the slant range plane be the defined image plane into which the samples of the range-compressed signals are back-projected. The operation of the global backprojection (GBP) algorithm is expressed by

$$h(\xi,\rho) = \int_{-\tau_0/2}^{\tau_0/2} S_{\mathrm{IF}}(\xi,f)\mathrm{e}^{-\mathrm{j}4\pi f_{\min}\tilde{R}/\mathrm{c}_0}\,\mathrm{d}\tau. \tag{9}$$

Here, the reconstructed SAR scene $h(\xi,\rho)$ is formed by the superposition of acquired range-compressed data S_{IF} and its corresponding backprojection into the defined image plane, τ_0 is the integration time, and $\tilde{R}$ the range distance calculated for the aperture position defined by $v\tau$ and the given azimuth ξ and range ρ in the defined image plane.

However, FMCW radars operate with discrete time signals. Thus, the backprojection algorithm for discrete-time sequences can be reformulated with a sum instead of an integral as

$$h(\xi,\rho) = \sum_{m_{\mathrm{a}}=1}^{M_{\mathrm{a}}} S_{\mathrm{int}}[m,\tilde{R}_{\mathrm{p}}], \tag{10}$$

where $m_{\mathrm{a}} = 1, \ldots, M_{\mathrm{a}}$ denotes the number of corresponding aperture positions and $\tilde{R}_{\mathrm{p}}$ is the range distance for the signal's trip from the FMCW SAR antenna aperture to the point in the defined image plane. Here, S_{int} denotes a complex-valued parameter estimated via the extended sinc interpolator introduced in [13]

$$S_{\mathrm{int}}[m, \tilde{R}_{\mathrm{p}}] = \sum_{i=n-L}^{n+L} \tilde{S}[m,i] w[i] \operatorname{sinc}\left[\frac{\pi(\tilde{R}_{\mathrm{p}} - \tilde{R}[i])}{\delta \tilde{R}}\right], \tag{11}$$

where

$$\tilde{S}[m,i] = S[m,i] \mathrm{e}^{\mathrm{j}4\pi f_{\mathrm{c}}(\tilde{R}_{\mathrm{p}} - \tilde{R}[i])/\mathrm{c}_0}. \tag{12}$$

Here $\tilde{S}[m,i]$ denotes the data samples involved in the interpolation procedure, the phase of which contains similar information about the assigned range distance R_{p}, f_{c} is the frequency emitted at $t = T/2$, and

$$S[m,n] = \frac{1}{N} \mathrm{FFT}\{s_{\mathrm{IF}}[m,n]\} \mathrm{e}^{-\mathrm{j}4\pi f_{\min} \tilde{R}[n]/\mathrm{c}_0} \tag{13}$$

for $n \in [0, N-1]$, where $N = f_{\mathrm{s}} T$ is the length of the sample sequence, and the phase correction term depends on the frequency $f_{\min}$ at $t = 0$.

III. Autofocusing

In practice, modern FMCW SAR systems, which operate at THz frequencies and can potentially be mounted on UAV platforms, can be sensitive to phase errors due to path deviation, e.g., caused by platform vibrations. If the path deviation information is known, it can be naturally included in the GBP algorithm that contains the motion-error compensation procedure. However, if the path deviation is unknown, an additional autofocusing procedure has to be involved, especially the one that can be incorporated into the image formation algorithm.

In the presence of path deviation of the SAR platform, the actual range distance between the platform and the scatterer in the scene under illumination can be expressed as

$$\begin{aligned} R_{\mathrm{act}} &= \sqrt{(v\tau + \Delta\xi'(\tau) - \xi)^2 + (\rho' + \Delta\rho'(\tau) - \rho)^2} \\ &\approx R + \frac{v\tau - \xi}{R}\Delta\xi'(\tau) + \frac{\rho' - \rho}{R}\Delta\rho'(\tau) = R + \Delta R(\tau), \end{aligned} \tag{14}$$

where R denotes the range distance estimated for the ideal path by (3), and ΔR the path deviation containing errors in the azimuthal $\Delta\xi'(\tau)$ and range directions $\Delta\rho'(\tau)$ for given aperture position at azimuth time τ. Consequently, the path deviation causes phase errors. The phase errors can be included in the representation of the reconstructed SAR scene by

$$h(\xi, \rho) = \sum_{m_{\mathrm{a}}=1}^{M_{\mathrm{a}}} S_{\mathrm{int}}[m, \tilde{R}_{\mathrm{p}}] \mathrm{e}^{\mathrm{j}\phi(m_{\mathrm{a}})}, \tag{15}$$

where $\phi(m_{\mathrm{a}})$ is the phase error due to platform path deviation for given azimuth time τ. Note that the phase errors are contained in the transformed IF signal (5) and, consequently, in the phase-controlled samples (12) used under the interpolation procedure. To restore an accurate SAR image reconstruction, the phase errors ϕ have to be estimated and eliminated.

Consider a single range bin of the reconstructed SAR image h for a fixed range ρ. Each pixel of the reconstructed image over the given bin is obtained based on the GBP algorithm (10) using the sinc interpolation procedure (11), and mathematically can be expressed as

$$\begin{aligned} h(m,\rho) = &\sum_{m_{\mathrm{a}}=1}^{M_{\mathrm{a}}} \sum_{i=n-L}^{n+L} \sigma[m_{\mathrm{a}}, \rho_i] w_i \\ &\times \operatorname{sinc}\left[\frac{\pi(R_{\mathrm{p}} - R[m_{\mathrm{a}}, \rho_i])}{\delta R}\right] \mathrm{e}^{\mathrm{j}4\pi f_{\mathrm{c}} R[m_{\mathrm{a}},\rho_i]/\mathrm{c}_0 + \mathrm{j}\phi(m_{\mathrm{a}})}, \end{aligned} \tag{16}$$

where $\phi(m_{\mathrm{a}})$ represents the phase error in the m_{a}-th observation, $\sigma[m_{\mathrm{a}}, \rho_i]$ is the reflectivity of the scatterer for the given aperture position at azimuth time τ and range ρ_i, δR is the difference between two consequent range samples. The formulation for each pixel (16) can also be rewritten in the matrix form as

$$\mathbf{h}(m,\rho) = \mathbf{\Phi}(m_{\mathrm{a}}, m_{\mathrm{a}}) \mathbf{a}(m, \rho_n) \mathbf{x}$$

where $\mathbf{\Phi} \in \mathbb{C}^{M_{\mathrm{a}} \times M_{\mathrm{a}}}$

$$\mathbf{\Phi} = \begin{bmatrix} \mathrm{e}^{\mathrm{j}\phi_1} & 0 & \ldots & 0 \\ 0 & \mathrm{e}^{\mathrm{j}\phi_2} & \ldots & 0 \\ \vdots & \vdots & \ddots & \vdots \\ 0 & 0 & \ldots & \mathrm{e}^{\mathrm{j}\phi(M_{\mathrm{a}})} \end{bmatrix}, \tag{17}$$

$\mathbf{a}(m, \rho_n) \in \mathbb{C}^{(2L+1)M_{\mathrm{a}} \times 1}$

$$\mathbf{a}(m, \rho_n) = \begin{bmatrix} \mathbf{b}_1 & \mathbf{b}_2 & \ldots & \mathbf{b}_{M_{\mathrm{a}}} \end{bmatrix}, \tag{18}$$

where $\mathbf{b}_{m_{\mathrm{a}}} \in \mathbb{C}^{(2L+1)\times 1}$

$$\mathbf{b}_{m_{\mathrm{a}}} = \begin{bmatrix} \mathrm{e}^{\mathrm{j}4\pi f_{\mathrm{c}} R[m_{\mathrm{a}},\rho_i]/\mathrm{c}_0} w_i \operatorname{sinc}\left[\frac{\pi(R_{\mathrm{p}} - R[m_{\mathrm{a}},\rho_i])}{\delta R}\right] \\ \vdots \\ \mathrm{e}^{\mathrm{j}4\pi f_{\mathrm{c}} R[m_{\mathrm{a}},\rho_i]/\mathrm{c}_0} w_i \operatorname{sinc}\left[\frac{\pi(R_{\mathrm{p}} - R[m_{\mathrm{a}},\rho_i])}{\delta R}\right] \end{bmatrix}^{\mathrm{T}}, \tag{19}$$

and $\mathbf{x} \in \mathbb{C}^{1 \times (2L+1)M_{\mathrm{a}}}$ contains reflectivities from scatterer σ for the corresponding range sample ρ_i and is expected to be sparse.

As a result, a range bin of the reconstructed SAR scene can be described by the following measurement linear model

$$\mathbf{h} = \mathbf{A}\mathbf{x} = \mathbf{\Phi}\mathbf{A}_1\mathbf{x}, \tag{20}$$

where $\mathbf{h} \in \mathbb{C}^{M \times 1}$

$$\mathbf{h} = \begin{bmatrix} \mathbf{h}(1,\rho) \\ \mathbf{h}(2,\rho) \\ \vdots \\ \mathbf{h}(M,\rho) \end{bmatrix}, \tag{21}$$

and $\mathbf{A}_1 \in \mathbb{C}^{M \times (2L+1)M_{\mathrm{a}}}$

$$\mathbf{A}_1 = \begin{bmatrix} \mathbf{a}(1,\rho) \\ \mathbf{a}(2,\rho) \\ \vdots \\ \mathbf{a}(M,\rho) \end{bmatrix}. \tag{22}$$

The compressed sensing theory provides a framework for the recovery of sparse signals [19]. Since M is far less than $(2L+1)M_{\mathrm{a}}$, it can be concluded that the sensing matrix $\mathbf{A}$ is underdetermined and well established to represent sparsely a SAR echo in the image plane for a given range ρ. Furthermore, the sensing matrix contains the phase errors ϕ. The compressed sensing theory provides the opportunity to recover $\mathbf{x}$ from measurement vector $\mathbf{h}$ by solving the following optimization problem

$$\begin{array}{ll} \text{minimize} & \|\mathbf{x}\|_0 \\ \text{subject to} & \|\mathbf{A}\mathbf{x}-\mathbf{h}\|_2 \leq \varepsilon, \end{array} \tag{23}$$

where $\|\cdot\|_0$ is the l_0 norm, which is the total number of non-zero elements in the vector. This problem is non-convex and requires computational resources to find an optimal solution. But it is possible to utilize the convex relaxation of (23) for sufficiently sparse $\mathbf{x}$ by solving the following optimization problem

$$\begin{array}{ll} \text{minimize} & \|\mathbf{x}\|_1 \\ \text{subject to} & \|\mathbf{A}\mathbf{x}-\mathbf{h}\|_2 \leq \varepsilon, \end{array} \tag{24}$$

where $\|\cdot\|_1$ denotes the l_1 norm, i.e. the sum of the absolute values of the vector's elements, and ε is the error tolerance. The problem can be solved via the CVX MATLAB software for disciplined convex programming [20], where the optimization is performed over $\mathbf{x}$, the solution to which will contain estimated reflectivities from scatterers $\sigma[m_{\mathrm{a}}, \rho_i]$ and phase errors ϕ. In this problem, for a known measured signal $\mathbf{h}$, an estimate of the reflectivities from the scattering objects in the scene under illumination $\mathbf{x}$ for a given range ρ is retrieved by time reversing $\mathbf{h}$ via the adjoint sensing matrix $\mathbf{A}^*$, so that the error tolerance can be chosen as

$$\varepsilon = \|\mathbf{h}-\hat{\mathbf{h}}\|_2 = \|\mathbf{h}-\mathbf{A}\mathbf{A}^*\mathbf{h}\|_2 = \|(1-\mathbf{A}\mathbf{A}^*)\mathbf{h}\|_2. \tag{25}$$

When the optimization problem (24) is solved, the phase errors can be determined separately as

$$\mathrm{diag}\{\mathbf{\Phi}\} = \mathbf{h} \quad (\mathbf{A}_1\mathbf{x}), \tag{26}$$

where denotes the Hadamard division. The optimization procedure is repeated iteratively with updated diagonal phase-error matrix $\mathbf{\Phi}$ for the sensing matrix $\mathbf{A} = \mathbf{\Phi}\mathbf{A}_1$ until the difference between two adjacent phase error estimates satisfies the required threshold

$$\epsilon_\Phi = \frac{\|\,\mathrm{diag}\{\mathbf{\Phi}\}_{l+1} - \mathrm{diag}\{\mathbf{\Phi}\}_l\|_2}{\|\,\mathrm{diag}\{\mathbf{\Phi}\}_l\|_2}, \tag{27}$$

where l denotes the iteration number of the optimization process.

Since the problem involves complex-valued parameters, it is reformulated to the optimization problem over the real-valued parameters as:

$$\begin{array}{ll} \text{minimize} & \|\mathbf{x}'\|_1 \\ \text{subject to} & \|\mathbf{A}'\mathbf{x}'-\mathbf{h}'\|_2 \leq \varepsilon, \end{array} \tag{28}$$

Table I: Measurement Setup Parameters

Parameter	Value
The lowest frequency processed, $f_{\min}$	$0.126\,\mathrm{THz}$
The highest frequency processed, $f_{\max}$	$0.182\,\mathrm{THz}$
Number of aperture positions, N_ξ	72
Speed of the platform, v	$4.11\,\mathrm{m/s}$
Ramp duration, T	$4.096\,\mathrm{ms}$
Duty cycle, $T+\Delta T$	$5\,\mathrm{ms}$
Reference distance, R_0	$\approx 2.335\,\mathrm{m}$
Integration angle, ϕ_0	$\approx 35^\circ$
Integration time, τ_0	$\approx 0.36\,\mathrm{s}$

where the sensing matrix, the measurement signal vector, and the sparse vector are represented as

$$\mathbf{A}' = \begin{bmatrix} \mathrm{Re}\{\mathbf{A}'\} & \mathrm{Im}\{\mathbf{A}'\} \\ \mathrm{Im}\{\mathbf{A}'\} & \mathrm{Re}\{\mathbf{A}'\} \end{bmatrix}, \tag{29}$$

$$\mathbf{h}' = \begin{bmatrix} \mathrm{Re}\{\mathbf{h}'\} \\ \mathrm{Im}\{\mathbf{h}'\} \end{bmatrix}, \tag{30}$$

and

$$\mathbf{x}' = \begin{bmatrix} \mathrm{Re}\{\mathbf{x}'\} \\ \mathrm{Im}\{\mathbf{x}'\} \end{bmatrix}, \tag{31}$$

respectively.

The algorithm for the phase-error estimation can be summarized as:

Algorithm 1: Algorithm for phase-error estimation ϕ

Task: Estimation of phase errors ϕ by solving (28)
Parameters: ρ, $\mathbf{A}_1$, $\mathbf{h}'$, tolerance μ
Initialization :
Let $\mathbf{\Phi}_{\mathrm{old}} = \mathbf{I}$, counter $c = 0$
LOOP Process
while $c < 6$ **do**
  $c = c + 1$, $\mathbf{A} = \mathbf{\Phi}_{\mathrm{old}}\mathbf{A}_1$, determine $\mathbf{A}'$ and ε
  Solve the optimization problem (28)
  Determine $\mathbf{x}$
  Estimate $\mathbf{\Phi}$ via (26) and update $\mathbf{\Phi}_{\mathrm{old}} = \mathbf{\Phi}$
  Calculate ϵ_Φ via (27)
  if $(\epsilon_\Phi \geq \mu)$ **then**
    $c = 0$
  end if
end while
Perform the phase correction for each range bin: $\mathbf{h}(\rho) = \overline{\mathrm{diag}\{\mathbf{\Phi}\}} \circ \mathbf{h}(\rho)$, where $\circ$ denotes the Hadamard product.

IV. Experimental Results

In this section, we consider the application of the proposed autofocusing algorithm that is fused as an add-on to the backprojection algorithm. The autofocusing algorithm is tested on the real data acquired through the outdoor FMCW SAR measurements at THz frequencies.

A. Measurement Setup

To evaluate the proposed autofocusing algorithm, an outdoor 2D monostatic SAR imaging was performed. In the experiment, the 2πSENSE FMCW radar operating in the D-frequency range $[0.126;\ 0.182]$ THz was mounted on a car; see Fig. 1. The length of the emitted frequency ramp was $T = 4.096\,\mathrm{ms}$, and a corner reflector, the object under test, was placed at the reference distance $R_0 \approx 2.335\,\mathrm{m}$. The duty cycle was set to $T + \Delta T = 5\,\mathrm{ms}$, and the average speed of the car was recorded as $v = 4.11\ \mathrm{m/s} = 14.8\,\mathrm{km/h}$ so that the SAR aperture step can be considered as $20.55\,\mathrm{mm}$. The SAR system operated in the scan mode. The acquired data demonstrated that only 72 azimuthal bins provide information that can be used to reconstruct the response of the object under test. Hence, the integration time $\tau_0 = 0.36\,\mathrm{s}$, and the corresponding integration angle based on reference distance and aperture length $v\tau_0$ is $\phi \approx 35^\circ$. All the measurement setup parameters are given in Table I.

B. Results

Figure 2a depicts the SAR scene reconstructed via the GBP algorithm (10). The scene contains degradation caused by the involvement of the start-stop-approximation principles in processing FMCW signals and the in-homogeneity of the SAR aperture caused by the non-uniform speed of the car, accelerations, and path deviations. In Fig. 2b is shown a SAR scene reconstructed with the backprojection algorithm and incorporated iterative compressed-sensing-based autofocusing algorithm (28), where the tolerance requirement is set to $\mu = 0.01$. The result demonstrates suppression of image degradation and target focusing. Hence, an autofocusing procedure in addition to the current image-formation algorithm is required.

To analyze the performance of the autofocusing algorithm, SAR scene cuts for fixed azimuth and range have been extracted; see Figs. 3a and 3b, respectively. Both the scene cuts are normalized with the peak intensity. It has been observed that the proposed algorithm does not affect the range profile of the SAR scene, as depicted in Fig. 3a. As a result, the $-3\,\mathrm{dB}$ range resolution remains $\Delta_\rho = 5.6\ \mathrm{mm}$. However, the autofocusing algorithm helps to improve the $-3\,\mathrm{dB}$ azimuthal resolution Δ_ξ from $6.1\ \mathrm{mm}$ to $4.4\ \mathrm{mm}$, which is about 27.9%. It can be concluded that the incorporation of the additional motion-error compensation procedure into the backprojection algorithm provides the opportunity to get an efficient THz SAR image-formation algorithm in the absence of information about path deviation.

Figure 1: Measurement setup.

V. Conclusions

In this paper, the autofocusing procedure based on the compressed-sensing approach (28) has been incorporated into the GBP algorithm (10) as an additional motion-compensation procedure. The proposed algorithm requires a single measured range bin as an input to estimate phase errors. The algorithm uses the advantages of the backprojection algorithm to construct the sensing matrix: the improved interpolation windowed sinc kernel, the range distances between the SAR platform and the points in the defined image plane, as a part of the convex-relaxed optimization problem. The performance of the algorithm has been tested on real data acquired through outdoor SAR imaging. The main conclusion is that the additional autofocusing-based motion-compensation procedure reduces the phase errors caused by speed variation, acceleration, and path deviation and improves the image reconstruction in terms of quality, e.g., an improvement of about 27.9% of the $-3\,\mathrm{dB}$ azimuthal resolution is obtained with the autofocusing approach.

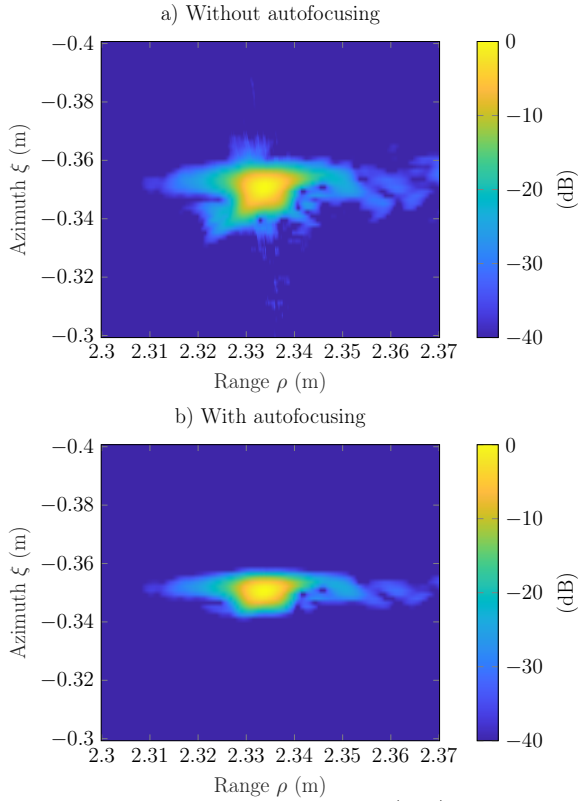

Figure 2: Reconstrcuted SAR scenes $h(\xi, \rho)$: a) without and b) with the proposed autofocusing procedure.

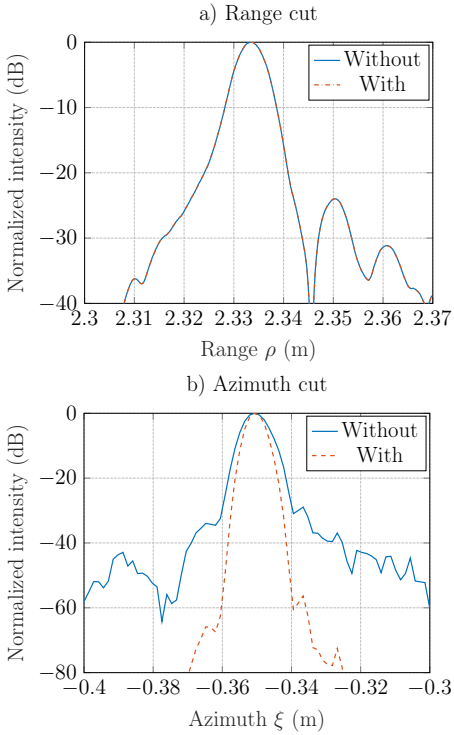

Figure 3: Evaluation of SAR scene cuts $h(\xi, \rho)$ subtracted from SAR images: a) for fixed azimuth $\xi = -0.351\,\mathrm{m}$; b) for fixed range $\rho = 2.33\,\mathrm{m}$.

Acknowledgment

The authors would like to acknowledge 2π-Labs GmbH for providing the radar system for data acquisition.

References

[1] M. Caris, S. Stanko, S. Palm, R. Sommer, A. Wahlen, and N. Pohl, "300 GHz radar for high resolution SAR and ISAR applications," in *2015 16th International Radar Symposium (IRS)*, Dresden, Germany, Jun. 24–26, 2015, pp. 577–580.

[2] Y. Zantah, F. Sheikh, A. A. Abbas, M. Alissa, and T. Kaiser, "Channel measurements in lecture room environment at 300 GHz," in *2019 Second International Workshop on Mobile Terahertz Systems (IWMTS)*, Bad Neuenahr, Germany, Jul. 1–3, 2019, pp. 1–5.

[3] A. Batra, V. T. Vu, Y. Zantah, M. Wiemeler, M. I. Pettersson, D. Goehringer, and T. Kaiser, "Sub-mm Resolution Indoor THz Range and SAR Imaging of Concealed Object," in *2020 IEEE MTT-S International Conference on Microwaves for Intelligent Mobility (ICMIM)*, Linz, Austria, Nov. 23, 2020, pp. 1–4.

[4] T. Bryllert, K. B. Cooper, R. J. Dengler, N. Llombart, G. Chattopadhyay, E. Schlecht, J. Gill, C. Lee, A. Skalare, I. Mehdi *et al.*, "A 600 GHz imaging radar for concealed objects detection," in *2009 IEEE Radar Conference*, Pasadena, CA, USA, 2009, pp. 1–3.

[5] S. Saqueb, N. Nahar, and K. Sertel, "Fast two-dimensional THz imaging using rail-based synthetic aperture radar (SAR) processing," *Electronics Letters*, vol. 56, no. 19, pp. 988–990, 2020.

[6] A. Batra, J. Barowski, D. Damyanov, M. Wiemeler, I. Rolfes, T. Schultze, J. C. Balzer, D. GÃ¶hringer, and T. Kaiser, "Short-Range SAR Imaging From GHz to THz Waves," *IEEE Journal of Microwaves*, vol. 1, no. 2, pp. 574–585, 2021.

[7] J. Schorlemer, C. Schulz, N. Pohl, I. Rolfes, and J. Barowski, "Compensation of sensor movements in short-range fmcw synthetic aperture radar algorithms," *IEEE Transactions on Microwave Theory and Techniques*, vol. 69, no. 11, pp. 5145–5159, 2021.

[8] S. Kueppers, T. Jaeschke, N. Pohl, and J. Barowski, "Versatile 126–182 GHz UWB D-band FMCW radar for industrial and scientific applications," *IEEE Sensors Letters*, vol. 6, no. 1, pp. 1–4, 2021.

[9] Y. Ivanenko, V. T. Vu, J. Barowski, H. Hellsten, and M. I. Pettersson, "Phase control in interpolation for backprojection of THz FMCW SAR signals," in *2022 23rd International Radar Symposium (IRS)*, Gdansk, Poland, Sep. 12–14, 2022, pp. 10–15.

[10] L.-E. Andersson, "On the determination of a function from spherical averages," *SIAM Journal on Mathematical Analysis*, vol. 19, no. 1, pp. 214–232, 1988.

[11] A. F. Yegulalp, "Fast backprojection algorithm for synthetic aperture radar," in *Proceedings of the 1999 IEEE Radar Conference. Radar into the Next Millennium (Cat. No. 99CH36249)*, Waltham, MA, USA, April 20–22, 1999, pp. 60–65.

[12] L. M. H. Ulander, H. Hellsten, and G. Stenström, "Synthetic-aperture radar processing using fast factorized back-projection," *IEEE Trans. Aerospace and Electronic Systems*, vol. 39, no. 3, pp. 760–776, 2003.

[13] Y. Ivanenko, V. T. Vu, A. Batra, T. Kaiser, and M. I. Pettersson, "Interpolation methods with phase control for backprojection of complex-valued SAR data," *Sensors*, vol. 22, no. 13, p. 4941, 2022.

[14] J. N. Ash, "An autofocus method for backprojection imagery in synthetic aperture radar," *IEEE Geoscience and Remote Sensing Letters*, vol. 9, no. 1, pp. 104–108, 2011.

[15] S. Wei, L. Zhou, X. Zhang, and J. Shi, "Fast back-projection autofocus for linear array sar 3-d imaging via maximum sharpness," in *2018 IEEE Radar Conference (RadarConf18)*, Oklahoma City, OK, USA, Apr. 23–27, 2018, pp. 0525–0530.

[16] A. Sommer and J. Ostermann, "Backprojection subimage autofocus of moving ships for synthetic aperture radar," *IEEE Transactions on Geoscience and Remote Sensing*, vol. 57, no. 11, pp. 8383–8393, 2019.

[17] J. Torgrimsson, P. Dammert, H. Hellsten, and L. M. Ulander, "Factorized geometrical autofocus for synthetic aperture radar processing," *IEEE Transactions on Geoscience and Remote Sensing*, vol. 52, no. 10, pp. 6674–6687, 2014.

[18] S. Shi, C. Li, J. Hu, X. Zhang, and G. Fang, "Study of phase error reconstruction and motion compensation for terahertz sar with sparsity-promoting parameter estimation," *IEEE Transactions on Terahertz Science and Technology*, vol. 11, no. 2, pp. 122–134, 2020.

[19] Y. C. Eldar and G. Kutyniok, *Compressed Sensing: Theory and Applications*. Cambridge University Press, 2012.

[20] M. Grant and S. Boyd, "CVX: A system for disciplined convex programming, release 2.0, ©2012 CVX Research, Inc., Austin, TX."